IEEE Access
Multidisciplinary | Rapid Review | Open Access Journal

Received 1 September 2022, accepted 3 November 2022, date of publication 7 November 2022, date of current version 15 November 2022.

Digital Object Identifier 10.1109/ACCESS.2022.3220688

RESEARCH ARTICLE

Simulation and Experimental Study of the Field Distribution of Engine for Electromagnetic Pulse

DONG ZHOU[1], MIN-XIANG WEI[2], JIE CAO[2], LIHUA SHI[1], (Member, IEEE), JINXING SHEN[1], AND LIZHOU AN[1]

[1]Army Engineering University of PLA, Nanjing 210016, China
[2]Nanjing University of Aeronautics and Astronautics, Nanjing 210016, China

Corresponding author: Min-Xiang Wei (dongzhouv576@nuaa.edu.cn)

ABSTRACT The protection of electromagnetic pulse (EMP) is important for aircraft due to vulnerable electronic equipments are installed. The control box of engine is also suffering from EMP and seldom studied. Meanwhile, most of work related to EMP protection focus on shielding design. Few works consider the effect of engine shell. The field distribution induced by EMP and its influences on the controller layout are unaddressed. This work will comprehensively investigate the field distribution characteristics of an engine under EMP, which is studied by simulating and experimenting methods. The transmission line matrix (TLM) is used to simulated field distribution of the bounded wave simulator and aero-engine, which provides better placement for equipment under test in the simulator. The field differences of bounded wave simulator and plane wave have been analyzed by using CST software. The feasibility of plane excitation instead of bounded wave simulator model excitation is checked, which has been verified by using the engine model. Then, the distribution characteristics of transverse and longitudinal fields surrounding the aero-engine are obtained, and the surface current distribution of the engine is also obtained in the simulation. The aero-engine simulation is excited by bounded wave simulator under CST software. According to the corresponding monitoring points, the simulated field distribution characteristics are verified by using the largely bounded wave simulator. Finally, the influence of field distribution on the layout of the engine electronic control system is analyzed, which provides a reference for the anti-electromagnetic pulse design of the engine electromagnetic controller.

INDEX TERMS Electromagnetic pulse (EMP), bounded wave simulator, placement for equipment under testing, field distribution of engine.

I. INTRODUCTION

Electromagnetic pulse (EMP) is one of the main damage effects of high-altitude nuclear explosion. The peak electric field of EMP can reach 10^5 V/m. Such a large pulse will induce severe changes in electromagnetic fields, thereby cause serious interference to cables, electronic equipment, etc. The aircraft is equipped with a large number of electronic and electrical equipment. These equipments are vulnerable to EMP. Thus, the susceptibility to EMP has been considered as a key issue for the certification of aircrafts [1].

Aero-engine is the most important component in the aircraft. The aero-engine is made of metals and operates in a mechanical principle. It will not be affected by EMP. However, the control system for the aero-engine can be easily destroyed by EMP, which can distort or even stop the aero-engine. Due to various considerations such as mass reduction, higher control complexity, regulation precision of different parameters, economic operation, etc. [2], [3], [4], modern aero-engine control systems are developed using low-voltage electronics that are vulnerable to EMP. Thus, the protection of control system becomes a main concern for aircraft manufacturers. Many researches focus on the reinforcement of electronic controller by using the shielded cables, shielded connectors, shielded cabinet and filters [5], [6], [7], [8], [9].

The associate editor coordinating the review of this manuscript and approving it for publication was Halil Ersin Soken.

However, few works consider the shielding effect of aero-engine shell. The field distribution induced by EMP and its influences on the controller layout are unaddressed.

The field distribution is an important factor for the arrangement of sensitive equipment, which can also improve the anti-interference ability of equipment with lower cost and less weight gain. The aero-engine exhibits a complex structure, which will cause great changes in the field distribution [10], [11]. It is favorable to place the sensitive device in places with less electromagnetic field.

This work will intensively investigate this issue through both simulation and experiment. Firstly, computational electromagnetic (CEM) tools can help predict the response of a complex structure. A wide variety of algorithms and methods have been developed to address the electrically large problems that are often encountered in the aircraft industry. We employ CST to simulation the 3D field distribution on the aero-engine. Then, the bounded wave simulator is used to test the aero-engine EMP coupling [12] for the experiment.

The rest of the paper is organized as follows: In Section II, the field differences of bounded wave simulator and plane wave have been analyzed by using CST software. Then the field and surface current distribution of aero-engine is simulated by using bounded wave simulator excitation. In Section III, the simulation of the electric field distribution on the aero-engine surface is verified by using the bounded wave simulator and the results from experiment agree well with our simulation results.

II. SIMULATION FIELD DISTRIBUTION OF ENGINE

In this chapter, the commercial full-wave simulation software, CST Microwave Studio, is used for analyzing the field distribution and the double exponential field signal effects in the bounded wave simulator. By comparing the standard double exponential wave with the field wave in bounded wave simulator, the advantages and disadvantages of using plane wave are analyzed for instead of bounded wave simulator model in simulation. Then, the optimal location is determined for EUT (equipment under test). At last, the surface field distribution of an aero-engine is simulated in the bounded wave simulator.

A. THE WAVEFORM OF EMP

With regard to the nuclear electromagnetic pulse, a double exponential function [13] is employed as the plane wave excitation source in numerical simulations.

$$E(t) = kE_p\left(e^{-\alpha t} - e^{-\beta t}\right). \tag{1}$$

where E_p is the peak value of the excitation, $k = 1/(e^{-\alpha t_p} - e^{-\beta t_p})$ a modifying factor to make $E/E_p = 1$ and t_p is the time for electric field rising to the peak. α and β are characteristic parameters satisfying the condition $\beta > \alpha > 0$, $t \geq 0$. The time domain waveform and the physical parameters are shown in figure 1(a)[14]. The spectrum of the excitation is computed by using Fourier transform and is shown in figure 1(b).

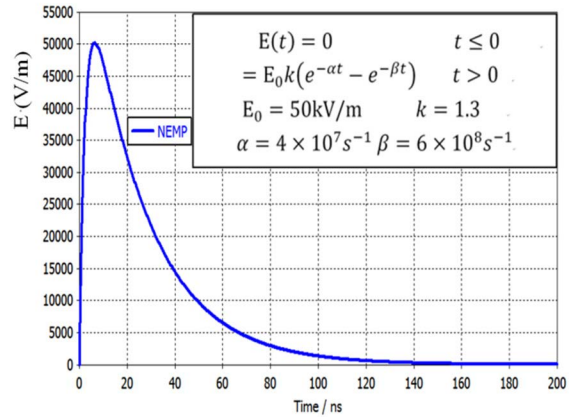

(a) Waveform in time domain

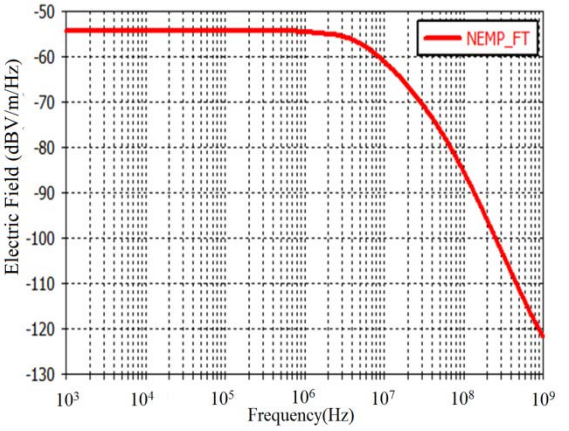

(b) Spectrum in frequency domain

FIGURE 1. The diagrams of nuclear electromagnetic pulses.

B. ANALYSIS OF FIELD IN BOUNDED WAVE SIMULATOR AND PLANE WAVE

The plane waves are used as excitation sources in CST Microwave Studio for the EMP (electromagnetic pulse) simulation. The volume of bounded wave simulator model is much larger than EUT, which greatly increase the software simulation time. And plane wave excitation provides standard double exponential wave in the simulation. However, the influence of bounded wave simulator is ignored on standard signal, which produces unacceptable tolerances.

The physical dimension of bounded wave simulator is shown as figure 2, and it is used to test surface field distribution of the aero-engine. The simulations are carried out by using the software CST [15]. To ensure high-precision simulation of open absorption boundaries and free space, "open (add space)" option is selected to automatically estimate the required space with "air" as background in the frequency range from 0 Hz to 600 MHz in this study [16].

The overall dimension of the simulator is 44 m×6 m×5 m, and the main geometric parameters are shown in the figure 2. The bounded wave simulator includes front tapered transition, parallel segment and rear tapered transition. The total length of the bounded wave simulator is 44 m with a

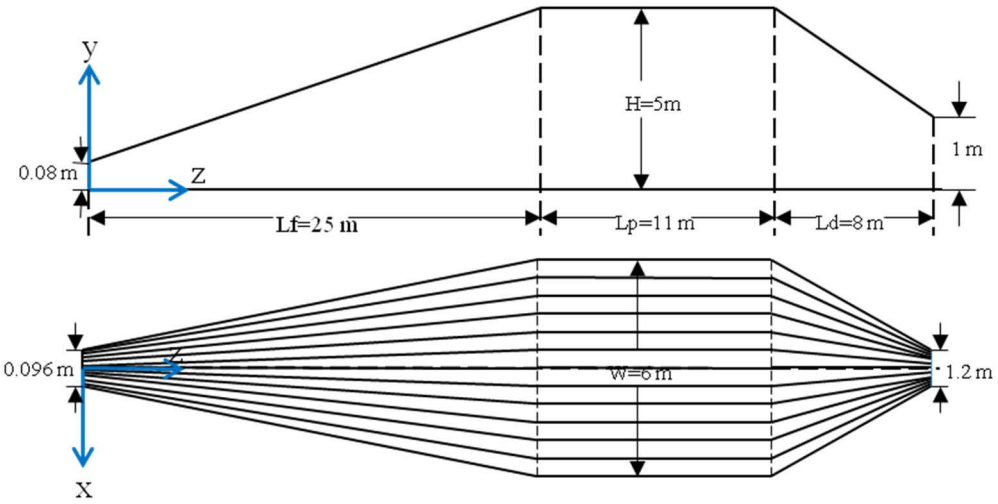

FIGURE 2. Structural dimension drawing of bounded wave simulator.

height and width of 5 m and 6 m respectively. The termination load is connected to a resistance array (R=135 Ω) which is formed in parallel with three 405 Ω resistors. The upper transmission lines are evenly distributed with 26 metal wire grids, which have a diameter of 3 mm. and the lower transmission line is consisted of a metal plate. In the simulation, the termination load is set up by three parallel "Lumped Element".

A typical double-exponential expression of early-time HEMP is adopted in figure 1(a), and the "Discrete Port" is used as the simulator excitation in software CST [17]. The simulation of the field distribution and field waveform of the bounded-wave simulator is performed.

As mentioned, plane wave is usually used as the excitation source of electromagnetic pulse coupling simulation. Although this setting can improve simulation efficiency, the influence of the bounded wave simulator on the field signal is ignored, which leads big tolerance values between the simulation and the experiments. As shown in figure 3, the electric field waveforms of bounded simulator are compared with standard waveform in time and frequency domains. Figure 3(a) shows that the amplitude of vertical electric field is higher than 50 kV/m in the working volume of bounded-wave simulator in time domain. The comparison of vertical field and total field shows that the bounded wave simulator has good field directionality in the vertical direction. Little difference is present in the time domain between rise times. The field amplitude drops rapidly in the descending region. And the spectrum shows the difference clearly in figure 3(b). When the frequency is less than 20 MHz, the field in the bounded wave is 3 dB smaller than the standard field. However, the field frequency is consistent between 20 MHz and 300 MHz.

The test parameter and tolerance values of nuclear electromagnetic pulse waveform have been shown in the military and civil test standards [18], as summarized in table 1. It shows that waveforms in the bounded wave simulator meet the requirements of the standards. In order to improve the matching accuracy of simulation and test, several points are suggested:

TABLE 1. Waveform parameters and tolerance standard of EMP.

	IEC 61000-4-25		VG 95371-10	VG 96903-50
	Test parameter	Tolerance value	Test parameter	Tolerance value
E_0	50kV/m	0-+6dB	50kV/m	±10%
10%-90%	2.5ns	±1.5ns	2.5ns	±10%
T_{FWHM}	25ns	25-75ns	23ns	±20%

(1) The test value is less than the values simulated by plant wave in low frequency (below 20 MHz). In order to ensure the reliability of equipment sensitive to low frequency region, the field amplitude should be increased properly in the bounded wave simulator.

(2) When the sensitive area of the tested equipment is located between 20 MHz and 300 MHz, plane wave can be used as excitation source instead of adding bounded wave simulator model. Because of the field waveform has a better consistency in this frequency region. All of this setting improves the simulation efficiency significantly.

(3) If the tested equipment is sensitive to overall frequency band, the amplitude of field strength in time domain should be increased properly. It makes the

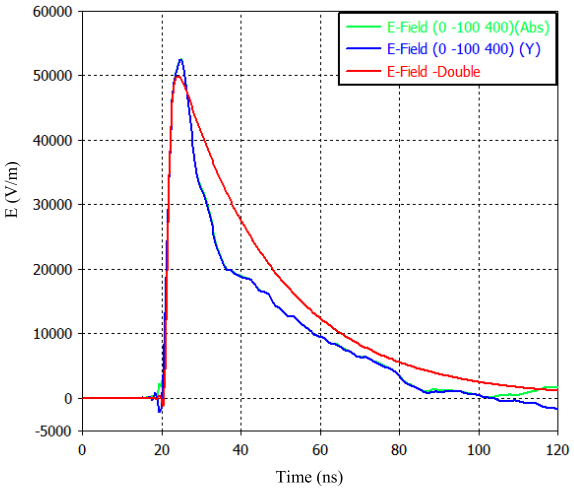

(a) Waveform in time domain

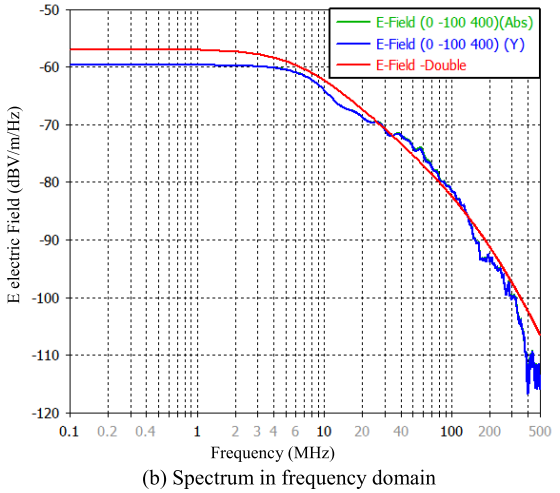

(b) Spectrum in frequency domain

FIGURE 3. Time and frequency domain waveforms of electric field.

field waveform closer to the standard waveform as a whole.

As the analysis showing, one has to tailor the plane wave usage according to his own range of interests.

E-field distribution inside the bounded-wave simulator is an important factor to ensure the field uniformity on the tested equipment. For getting a better testing result, the optimal test location should be selected in the bounded wave simulator. Figure 4 shows the E-field distribution inside the bounded-wave simulator at t=147 ns. At this moment, the wave just arrives to the end of the simulator. And figure 4 shows the largest electric field amplitude at the back of the simulator. The E-field distribution at both ends is worse than the middle parallel section, which is effected by the terminal load and pulse source. The front end of parallel section has a better field uniformity than other places. Also the field in the middle is slightly larger than both sides. From the discussion above, the tested equipment should be located in the front end of parallel section. And it is supported by the insulated object for leaving a certain distance from lower metal plate.

C. SIMULATION OF ELECTROMAGNETIC FIELD DISTRIBUTION ON AERO-ENGINE SURFACE

With the development of electronic control technology, the complexity of the aero-engine control system is ever-increasing. The control system is more susceptible to EMP effects. Then, the ability of the aero-engines to resist electromagnetic pulse interference becomes a popular research in recent years. The field distribution of aero-engine is an important factor for the arrangement of sensitive equipment, which can also improve the anti-interference ability of equipment with lower cost and less weight gain. The surface field distribution of aero-engine is simulated using full wave algorithm in CST software, which is excited by bounded wave model excitation. The difference of plane wave and bounded wave model excitation is compared based on the special point field. For reducing the tolerance between simulation and experiment, bounded wave model excitation is used for field distribution simulation of aero-engine.

To obtain the differences of plane wave and bounded wave model excitation, two models have been developed in CST including the aero-engine geometry model. The geometry of aero-engine is shown in figure 5, which includes the reduction gearbox, air inlet, accessones gearbox, combustor, power turbines and exhaust pipe. The dimensions are 2.5 m long, 0.75 m wide and 0.82 m high. The points of P1, P2, P3, P4 are the field detection points in the simulation. In the simulation of bounded wave model excitation, boundary condition is identical to that of bounded wave simulation, which includes the setting of excitation source. According to the above field simulation of bounded wave simulator, the aero-engine is located in the front of parallel section, as shown in figure 6(a). The aero-engine has a distance of 27 meters from the pulse source, 1 meter from the lower flat transmission line and transverse symmetrical distribution in simulator. For the plane wave excitation model, the standard double exponential pulse signal is added as shown in figure 1(a). To obtain the high-precision simulation of open absorption boundaries and free space, ''open (add space)'' option is used to automatically estimate the required space, with ''air'' as the background, and frequency range is defined from 0 Hz to 600 MHz. Identical propagation direction was used for both simulations, as shown in figure 6(b). All materials of aero-engine are set to ''PEC'' to speed up the simulation.

The comparison between plane wave and bounded wave model is shown in figure 7(a) for time domain and frequency domain. The fields from point P3 (figure 5) are chosen. The figure 7(a) shows the comparison in time domain. And figure 7(b) is the comparison in frequency domain. In time domain, the rise time is almost constant with noticeable delay due to the propagation length difference. In frequency domain, when the frequency below 20 MHz, the field amplitude of plane wave excitation is about 3 dB

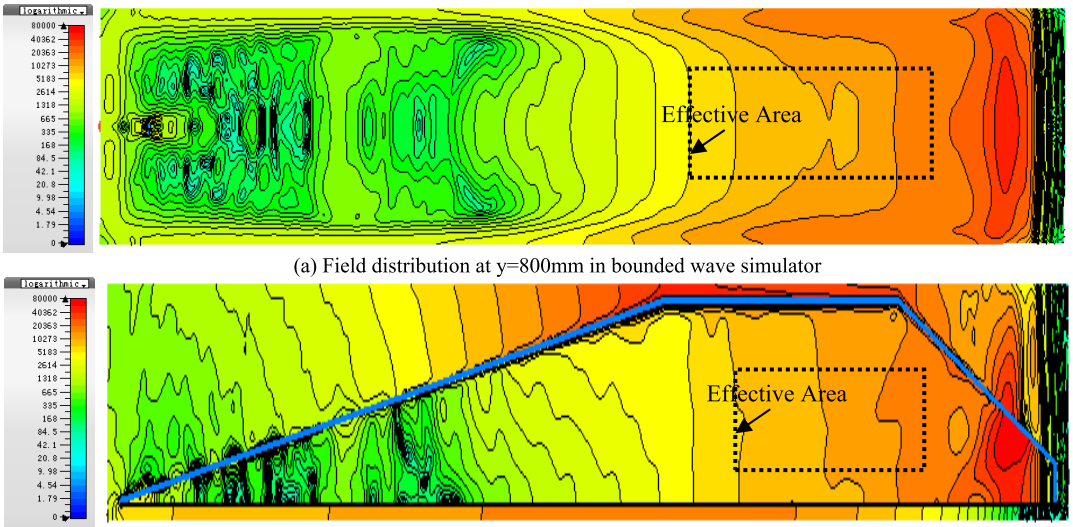

(a) Field distribution at y=800mm in bounded wave simulator

(b) Field distribution at x = 0 in bounded wave simulator

FIGURE 4. Distribution of vertical E-field in bounded-wave simulator.

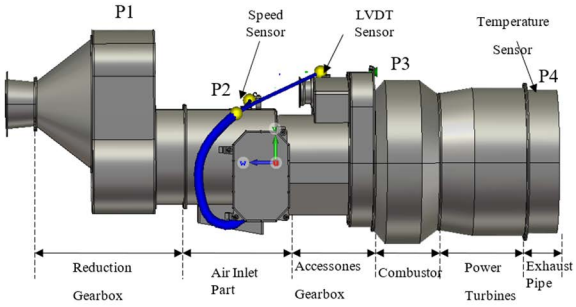

FIGURE 5. Diagram of aero-engine structure.

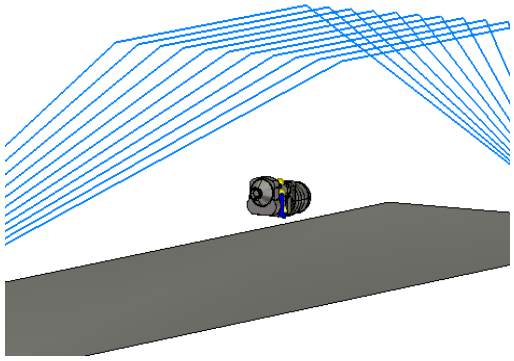

(a) Simulation model of engine excited by bounded wave simulator

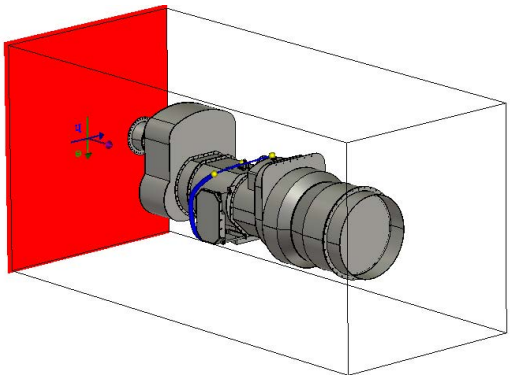

(b) Simulation model of engine excited by plane wave

FIGURE 6. EMP simulation model of engine.

higher than that of bounded wave model excitation. However, it is very consistent from 20 MHz to 400 MHz. All of this analysis is consistent with the above results as in section II B. In order to reduce the tolerance of simulation and experiment, all of the following simulation results are obtained from the bounded wave model excitation. ield comparison of bounded wave simulator and plane wave excitation.

The simulation results of detection points around aero-engine are shown as figure 8 and figure 9. Figure 8 shows the time domain and frequency domain results of transverse field changes in the monitoring point P1. Due to the influence of surface current, field strength decreases with distance increasing from aero-engine surface. Then the wiring harness shall be arranged with a certain distance from aero-engine and supported by a support frame. The frequency domain shows that the difference of coupling below 200 MHz, which proves that the main coupling frequency band of EMP is below 200 MHz. Both time domain and frequency domain have the same waveform excepting for the amplitude.

Taking account of the surface electric field distribution, the field of four representative points was selected for analyzing the longitudinal field distribution. The monitoring point locations are shown in figure 5. And the results are shown as

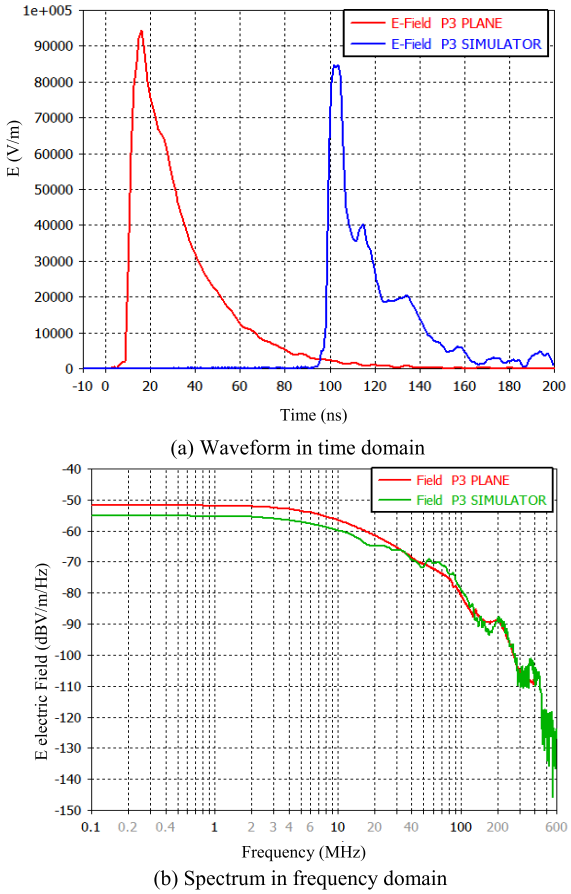

FIGURE 7. Field comparison of bounded wave simulator and plane wave excitation.

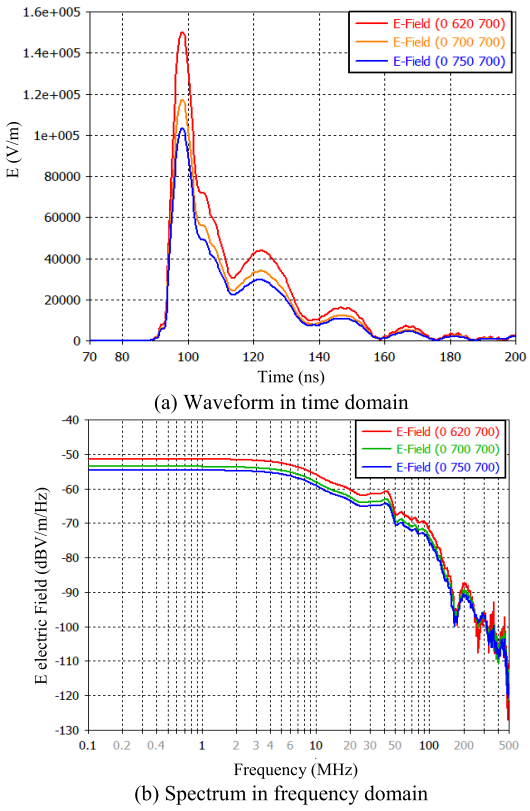

FIGURE 8. Field distribution on transverse surface of engine.

figure 9. In contrast to the transverse field, the longitudinal field varies greatly in amplitude. From the time domain in the figure 9(a), the field amplitude is changed from 40 kV/m to 115 kV/m, and the field amplitude of P2 is smaller than that of P1. The frequency domain of figure 9(b) shows that the coupling frequency varies for different points. All of the coupling frequency is, nevertheless, lower than the 200 MHz.

The two-dimensional electric field distribution of aero-engine is shown in the figure 10. The longitudinal two-dimensional electric field distribution of aero-engine is shown in the figure 10(a). Figure 10(b) shows the two-dimensional transverse field distribution at the monitoring point P1. Figure 10(c) shows the two-dimensional transverse field distribution at the monitoring point P2. Figure 10(d) shows the two-dimensional transverse field distribution at the monitoring point P3. The large amplitude of electric field mainly appears above and below the aero-engine. Then, weak field strength appears at left and right sides. Compared with the figure 5, upper and lower part of reduction gearbox has the large amplitude of electric field. And the electric field amplitude of air inlet is lower than the amplitude of incident electric field. The field amplitude of exhaust pipe is higher. The surface current distribution of aero-engine is shown as in figure 11.

III. EXPERIMENT OF ELECTROMAGNETIC FIELD DISTRIBUTION ON ENGINE SURFACE

The electric field distribution on the aero-engine surface is verified by using the bounded wave simulator. The surface material of aero-engine has good conductivity. And the saturation and nonlinearity are not considered, which are believed to be less important in our study. Then weak field expansion of instead of strong field test is used here without loss of generality.

In the experiment, the equal-probability aero-engine model was built for real aero-engine with the material 304 stainless steel with good conductivity. The aero-engine model has dimension of 2.5 m long, 0.75 m wide and 0.82 m high. The real aero-engine model is shown in figure 12. The aero-engine model is located in the bounded wave simulator as described in the simulation. It has a distance of 27 meters from the front surface of the aero-engine model to the pulse source, 1 meter from the lower flat transmission line and transverse symmetrical distribution in the simulator. The aero-engine model should be supported from the flat transmission line by insulating support. The geometry of the bounded wave simulator is similar with the bounded wave simulator simulation. And the field uniformity of the simulator has been proved several times. Due to the limitation of the number of electric field probes, three simulation monitoring points are verified in this experiment. The locations of electric field probes are shown in figure 12. Probe coefficient after calibration is listed

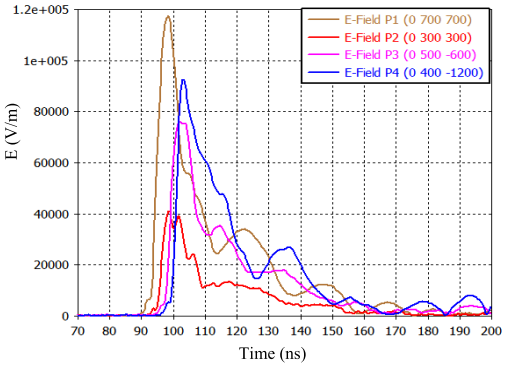

(a) Waveform in time domain

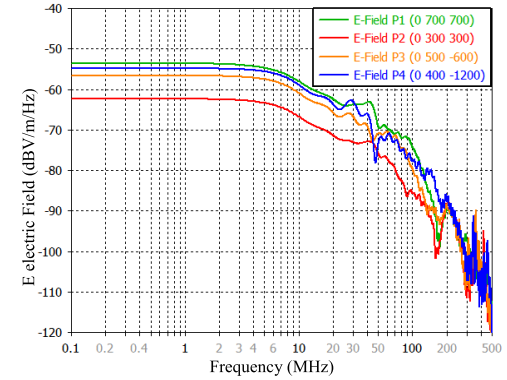

(b) Spectrum in frequency domain

FIGURE 9. Field distribution on longitudinal surface of engine.

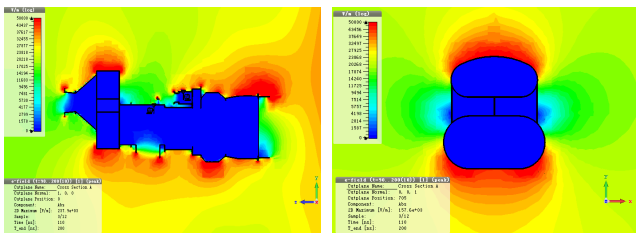

(a) Longitudinal field distribution of engine (b) Transverse field distribution of reduction gearbox

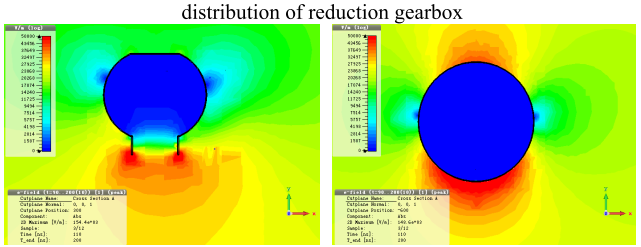

(c) Transverse field distribution of air inlet (d) Transverse field distribution of reduction combustor

FIGURE 10. Two-dimensional electric field distribution of engine.

in Table 2. In order to reduce the electromagnetic interference, all signals of the electric field probes are transmitted through optical fiber to the shielding room.

When the bounded wave simulator operates without the aero-engine model, the electric field waveform is shown in figure 13(a). The field amplitude is 300 V/m. The result

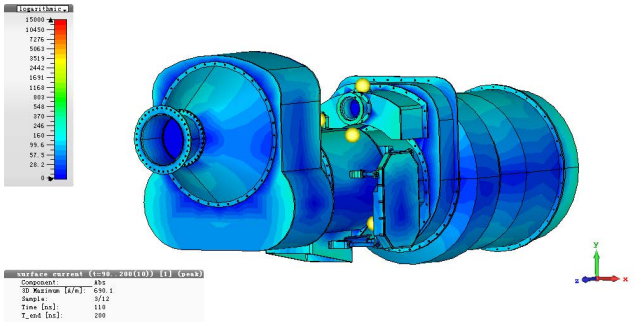

FIGURE 11. Surface current distribution of engine.

FIGURE 12. Experiment layout of engine model.

TABLE 2. Waveform parameters and tolerance standard of EMP.

Probe position	Probe coefficient (V/m/V)
P1	450
P2	340
P3	333

TABLE 3. Proportion of electric field at monitor point.

Point	Simulation results	Testing results
1	115 kV/m	540 V/m
2	40 kV/m	230 V/m
3	75 kV/m	390 V/m
Ratio	2.87:1:1.87	2.35:1:1.7

from the testing point of the aero-engine model is shown in figure 13(b). The results show that the waveform of testing points is still a double exponential waveform. Then the amplitude varies greatly at different points. At testing point P1, the amplitude of electric field is up to 540 V/m. The amplitude of electric field is about 390 V/m at point P3. The minimum amplitude of electric field appears in the point P2, which is about 230 V/m. The proportion of electric field at monitor point shows that the simulation and test results have the same field distribution trend. The rate of simulation is that P1:P2:P3=2.87:1:1.87. The test result is about P1:P2:P3=2.35:1:1.7. The tolerance may be produced by the height of the electric field probe. At the same time, the tolerance will be amplified by weak field test of 300 V/m. However, this test also proves that the simulation and field

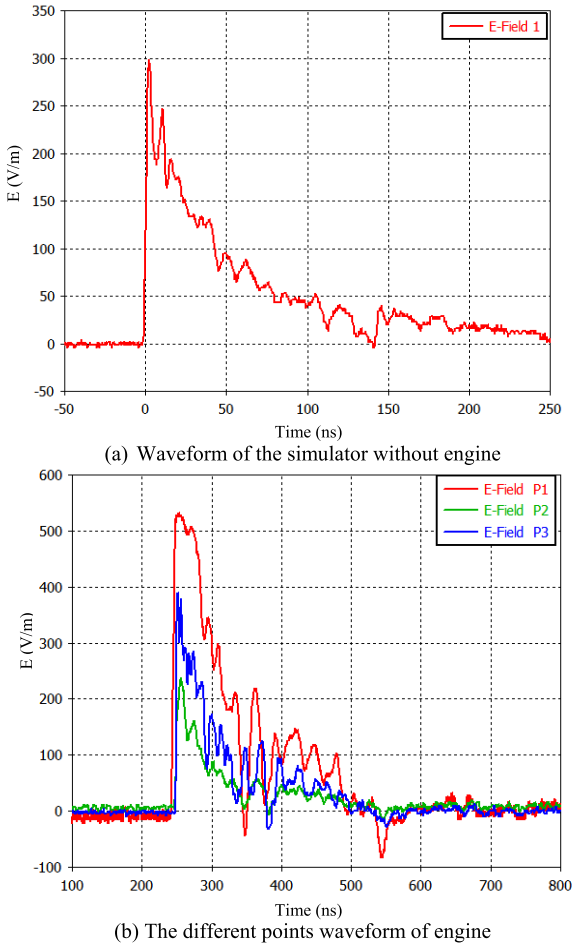

(a) Waveform of the simulator without engine

(b) The different points waveform of engine

FIGURE 13. Test result waveform.

distribution are corrected. Then, there is another problem that whether the weak field experiment can verify the strong field distribution. The linear field characteristics of metal surface has been verify by last experiment. Based on the results, the sensitive equipment should be located in the low amplitude field region.

IV. CONCLUSION

In this paper, simulation shows that plane wave excitation can be used as bounded wave simulator excitation in EMP simulation. And the E-field distribution at both ends is worse than the middle parallel section, which is affected by the terminal load and pulse source. The front end of parallel section has a better field uniformity than other places, which provide the reference for the location of engine in the bounded wave simulator. Then, the field amplitude of plane wave excitation is slightly higher than that of bounded wave excitation. Then the fields have a good consistency in frequency between 20 MHz and 300 MHz. When the frequency is less than 20 MHz, the field in the bounded wave is 3 dB smaller than the standard field.

The protection of electromagnetic pulse (EMP) is important for aircraft due to vulnerable electronic equipments are installed. The control box of engine is also suffering from EMP and seldom studied. Meanwhile, few works consider the effect of engine shell. The research shows that serious uneven field distribution appears on the aero-engine surface. It will be a good idea that reasonable arrangement of sensitive equipment is used to increase ant-interference capability. The simulation and experiment show that the upper field amplitude of reduction gearbox is 150 kV/m. The electric field amplitude of air inlet, lower than the amplitude of incident electric field, is only about 40 kV/m. According to the electrical field of monitoring points, the experiment has been conducted in the bounded wave simulator. The simulation is proved by using the method of field rate. The proposed method will improve the ability of resisting HEMP for the design of aero-engine electronic control system.

ACKNOWLEDGMENT

The authors would like to thank project funding for all of the work in this manuscript. It also includes Zheng Sun for experiment support and checking this article.

REFERENCES

[1] N. J. Carter, "The past, present and future challenges of aircraft EMC," *IEEE Electromagn. Compat. Mag.*, vol. 1, no. 1, pp. 75–78, 1st Quart., 2012.

[2] K. Beneda, "Development of a modular FADEC for small scale turbojet engine," in *Proc. IEEE 14th Int. Symp. Appl. Mach. Intell. Informat. (SAMI)*, Jan. 2016, pp. 51–56.

[3] V. M. Novichkov and A. Y. Burova, "Algorithm of two turbojets thrust asymmetry minimization for digital control system of twin-engine jet airliner," in *Proc. Int. Multi-Conf. Ind. Eng. Modern Technol. (FarEastCon)*, Oct. 2019, pp. 1–6.

[4] X. Zhang and R. Zhang, "Study on the construction of the pricing parameter model of aero engine digital control system test," in *Proc. Int. Conf. Netw., Commun. Inf. Technol. (NetCIT)*, Dec. 2021, pp. 276–280.

[5] S. A. Pignari and G. Spadacini, "Plane-wave coupling to a twisted-wire pair above ground," *IEEE Trans. Electromagn. Compat.*, vol. 53, no. 2, pp. 508–523, May 2011.

[6] E. B. Savage, W. A. Radasky, and R. Willliamson, "Time domain measurement of shielded cables with connectors," in *Proc. IEEE Int. Symp. Electromagn. Compat. (EMC)*, Jul. 2016, pp. 148–152.

[7] A. Rabat, P. Bonnet, K. E. K. Drissi, and S. Girard, "An analytical evaluation of the shielding effectiveness of enclosures containing complex apertures," *IEEE Access*, vol. 9, pp. 147191–147200, 2021.

[8] Y. Chen, Q. Liu, W. Yan, C. Zhu, Y. Zhao, and B. Yu, "Research on EMI noise suppression method based on electromagnetic shield of cabinet," in *Proc. PURPLE MOUNTAIN FORUM Int. Forum Smart Grid Protection Control*. Cham, Switzerland: Springer, 2020, pp. 905–921.

[9] Z. Yan, F. Qin, J. Cai, S. Zhong, and J. Lin, "Shielding performance of materials under the excitation of high-intensity transient electromagnetic pulse," *IEEE Access*, vol. 9, pp. 49697–49704, 2021.

[10] G. G. Gutierrez, S. F. Romero, M. Gonzaga, E. Pascual-Gil, L. D. Angulo, M. R. Cabello, and S. G. Garcia, "Influence of geometric simplifications on lightning strike simulations," *Prog. Electromagn. Res. C*, vol. 83, pp. 15–32, 2018.

[11] G. G. Gutierrez, S. F. Romero, M. Gonzaga, E. Pascual-Gil, L. D. Angulo, M. R. Cabello, and S. G. Garcia, "Influence of geometric simplifications on high-intensity radiated field simulations," *Prog. Electromagn. Res. C*, vol. 86, pp. 217–232, 2018.

[12] B.-L. Nie, P.-A. Du, and P. Xiao, "An improved circuital method for the prediction of shielding effectiveness of an enclosure with apertures excited by a plane wave," *IEEE Trans. Electromagn. Compat.*, vol. 60, no. 5, pp. 1376–1383, Oct. 2018.

[13] N. Mora, B. Daout, M. Nyffeler, C. Romero, and F. Rachidi, "Revisiting the calculation of the early time HEMP conducted environment," *IEEE Trans. Electromagn. Compat.*, vol. 63, no. 1, pp. 111–124, Feb. 2021.

[14] *FORCE, AIR, and Air Force Sustainment Center-Oklahoma City*, document MIL-STD-461F, 2007.
[15] *CST Studio Suite Help*, CST GmbH, Waldshut-Tiengen, Germany, 2008.
[16] L. Yao, T. Shen, N. Kang, D. Liu, and J. Huang, "Time-domain simulation and measurement of a guided-wave EMP simulator's field uniformity," *IEEE Trans. Electromagn. Compat.*, vol. 55, no. 6, pp. 1187–1194, Dec. 2013.
[17] C. Wang, J. Li, A. Zhang, W. T. Joines, and Q. H. Liu, "Dual-band capacitively loaded annular-ring slot antenna for dual-sense circular polarization," *J. Electromagn. Waves Appl.*, vol. 31, no. 9, pp. 867–878, Jun. 2017.
[18] F. Sabath and S. Potthast, *Quality Criteria for NEMP Test Environments*. Edison, NJ, USA: IET, 2016.

DONG ZHOU received the doctorate degree from the School of Nanjing University of Aeronautics and Astronautics (NUAA), Nanjing, China, in October 2020. He is a Lecturer with Army Engineering University of PLA, Nanjing. His research interest incudes coupling mechanism of engine strong electromagnetic pulse.

MIN-XIANG WEI received the Ph.D. degree in vehicle engineering from Xian Jiaotong University, Xian, China, in March 2001. He is a Professor of energy and power with the Nanjing University of Aeronautics and Astronautics. His research interests include vehicle electronics and automation, aviation piston engine electronic control, vehicle safety control, and electric vehicle control technology.

JIE CAO received the B.S. degree in vehicle engineering from the Inner Mongolia University of Technology, Hohhot, China, in July 2017. He is currently pursuing the Ph.D. degree with the Nanjing University of Aeronautics and Astronautics, Nanjing. His research interests include the development and implementation of forced electromagnetic pulse coupling and protection technologies for aeroengine control systems.

LIHUA SHI, photograph and biography not available at the time of publication.

JINXING SHEN, photograph and biography not available at the time of publication.

LIZHOU AN, photograph and biography not available at the time of publication.